



UNIVERSITY OF LEEDS

This is a repository copy of *Controlled comparison of machine vision algorithms for Rumex and Urtica detection in grassland*.

White Rose Research Online URL for this paper:
<http://eprints.whiterose.ac.uk/117717/>

Version: Accepted Version

Article:

Binch, A and Fox, CW orcid.org/0000-0002-6695-8081 (2017) Controlled comparison of machine vision algorithms for Rumex and Urtica detection in grassland. *Computers and Electronics in Agriculture*, 140. pp. 123-138. ISSN 0168-1699

<https://doi.org/10.1016/j.compag.2017.05.018>

© 2017, Elsevier. Licensed under the Creative Commons Attribution-NonCommercial-NoDerivatives 4.0 International
<http://creativecommons.org/licenses/by-nc-nd/4.0/>

Reuse

Items deposited in White Rose Research Online are protected by copyright, with all rights reserved unless indicated otherwise. They may be downloaded and/or printed for private study, or other acts as permitted by national copyright laws. The publisher or other rights holders may allow further reproduction and re-use of the full text version. This is indicated by the licence information on the White Rose Research Online record for the item.

Takedown

If you consider content in White Rose Research Online to be in breach of UK law, please notify us by emailing eprints@whiterose.ac.uk including the URL of the record and the reason for the withdrawal request.



eprints@whiterose.ac.uk
<https://eprints.whiterose.ac.uk/>

Controlled comparison of machine vision algorithms for Rumex and Urtica detection in grassland

A Binch ^{a,c}, CW Fox ^{b,c}

^a School of Computing, ^b Institute for Transport Studies,
The University of Leeds, LS2 9JT, United Kingdom.

^c Ibex Automation Ltd, S35 7DQ, United Kingdom.

Corresponding author: C.W.Fox@leeds.ac.uk

Submitted to Computers and Electronics in Agriculture

May 16, 2017

Abstract

Automated robotic weeding of grassland will improve the productivity of dairy and sheep farms while helping to conserve their environments. Previous studies have reported results of machine vision methods to separate grass from grassland weeds but each use their own datasets and report only performance of their own algorithm, making it impossible to compare them. A definitive, large-scale independent study is presented of all major known grassland weed detection methods evaluated on a new standardised data set under a wider range of environment conditions. This allows for a fair, unbiased, independent and statistically significant comparison of these and future methods for the first time. We test features including linear binary patterns, BRISK, Fourier and Watershed; and classifiers including support vector machines, linear discriminants, nearest neighbour, and meta-classifier combinations. The most accurate method is found to use linear binary patterns together with a support vector machine.¹

¹This research was supported in part by the InnovateUK project IBEX2: Autonomous robot weed spraying for less favoured areas, grant number 131790.

1 Introduction

Automated robotic weeding of grassland will improve the productivity of dairy and sheep farms while helping to conserve their environments. At present grassland weeding is typically performed in two styles. Tractor-mounted bulk spraying of selective herbicides is expensive due to the volume, and cost per unit of selective chemicals. Manual backpack-mounted spraying uses lower, targeted spot spray doses of generic herbicides such as glyphosate, but requires more expensive manual labour time. Precision robots [4, 6] present an opportunity to use similarly low and targeted doses of cheap generic herbicides as in the manual case, but at much lower cost as they can drive, detect and spray automatically without the need to pay manual sprayers by the hour. Precision robots could further eliminate the need for chemical herbicide altogether by destroying detected weeds with mechanical or other non-chemical methods. Data collected about weed locations by robots can be fed into geospatial weed mapping systems to enable ecological analyses.

Autonomous weeding robots must first detect weeds at a suitable resolution and accuracy. Machine vision provides many tools and algorithms for detection, with varying performances, and can be cheap to operate using consumer-grade cameras. Several previous studies have reported results of machine vision methods to separate grass from grassland weeds, typically *Rumex obtusifolius* (dockleaf). But as is common in early stages of artificial intelligence research, they each use their own datasets and report only performance of their own algorithm rather than presenting controlled trials testing methods against one another. As proof of concept studies, many used only small data sets, did not report confidence intervals on their accuracy rates, and have not yet tested methods across lighting and weather conditions which are known to affect many vision algorithms. It is well known in artificial intelligence that unintended author bias and bottom drawer effects can creep into studies when the same author both designs and tests an algorithm, so there is a need for independent validation. We present a large-scale (tens of thousands of images), independent study of all major grassland weed detection methods evaluated on a new standardised data set, under a wider range of environment conditions. This allows for a fair, unbiased, independent and statistically significant comparison of the methods for the first time.

46 1.1 Previous work

47 Previous studies can be grouped roughly into those which classify individual windows (patches)
48 of images (e.g. tens of pixels square) independently of one another, and those which apply mor-
49 phological operations to whole images (e.g. hundreds or thousands of pixels width and height).
50 Window-based methods compute features of the windows such as spectra or texture descriptors,
51 while whole-image methods try to isolate shapes via segmentation algorithms. Window-based
52 methods include: [10] used local binary pattern (LBP) texture features with a per pixel threshold
53 Rumex/Grass classifier, under controlled artificial lighting conditions, to report between 87%-
54 97% accuracy on a test set of 941 images of 50x40 pixels. [2] uses very large windows to obtain
55 high accuracy, 98.5%, using texture features and support vector machine (SVM) classification.
56 Whole-image segmentation methods include: [12] segmented images into regions of similar tex-
57 ture then classified the shapes of these regions, reporting 71%-95% accuracy in Rumex/(Grass
58 and mixed herbs) classification under constant lighting conditions. [27] used thresholded and
59 segmented Fast Fourier Transforms (FFT) to detect Rumex in grass on 161 images, reporting
60 94% accuracy. [33] used a similar setup to report accuracies 82%-89% for Rumex/Grass. [31]
61 used segmentation (erosion and dilation). [17] use Gray Level Co-occurrence Matrix and Laws'
62 filter mask texture features with linear discriminant analysis (LDA) and segmentation to report
63 90% Rumex/Grass. [18] use Markov Random Field based texture features and segmentation to
64 report a 97.8% accuracy on 92 images. A summary of the key properties of each method is
65 given in table 1 (plant types are R=Rumex, G=Grass, U=Urtica, H=mixed herbs).

66

study	method	classes	reported accuracy	number of test images	illumination	window size
[10]	LBP+threshold	R/G	87%-97%	941	artificial	50×40
[12]	Segment+shape	R/(G+H)	71%-95%	3681 windows	constant	n/a
[27]	FFT+segment	R/G	94%	161 images	constant	8
[33]	FFT+segment	R/G	82%-89%	56 images	constant	8
[31]	Segment	R/G	89%	240 images	constant	n/a
[17]	GLCM+LDA+segment	R	90%	92 images	constant	n/a
[18]	MRF segment	R/G	97.8%	92 images	constant	n/a
[2]	LBP+SVM	R	98.5%	400 images	varied	320×240

67

68 From the table, it is clear that making a fair comparison of these algorithms is difficult
69 or impossible from publicly available data. Each study uses its own data sets, comprising
70 completely different images and conditions. In many cases the separation of training and test
71 data is not clear, with studies reporting best results having optimised parameters over the
72 same test set used in the final result, rather than making a clean train/test separation. It is
73 well-known [11] that optimising parameters to the test set tends to yield over-optimistic results
74 compared to performance on new data. Some studies do not describe the variation in the
75 lighting conditions, but are assumed to be constant conditions because they use small numbers
76 of test images collected, presumably, on the same day. Window-based methods have used
77 different window sizes, while whole-image segmentation methods make use of data from across
78 the whole image to classify each local pixel, which is hard to meaningfully evaluate against
79 windowed results. Window size is important because it represents a fundamental trade-off
80 between detection accuracy and spatial resolution. A large window contains more information
81 which will yield high accuracies, but at the cost of a lower spatial resolution, for example in
82 determining what area of ground to spray with herbicide.

83 In our native UK grassland, Rumex is not the only common weed and almost always co-
84 occurs with similar populations of *Urtica diotica* (stinging nettle). As such, any automated
85 grassland weeding system needs to work with both Rumex and Urtica together. If Rumex
86 only was precision sprayed, then a selective bulk spray for Urtica would still be needed which
87 negates the utility of the Rumex precision system, as combined Urtica and Rumex selective

88 chemicals are available. Previous work on automatic detection of *Urtica* in grassland has relied
89 on non-visual spectral methods including near infra-red and full hyper-spectra [23, 24, 38], but
90 these sensors are more costly than simple visual cameras. *Urtica* has smaller leaves than *Rumex*
91 which makes it harder to detect with machine vision alone, in particular some *Rumex* detection
92 methods rely entirely on obvious features of the large, smooth *Rumex* leaves, which may not
93 carry over to the *Urtica* case. However *Urtica* has distinctive jagged edges on its leaves which
94 suggest that methods based on such local shapes (rather than texture) features may be useful
95 for detection.

96 With the exception of [2], all the systems in table 1 rely on vertical camera angles, i.e.
97 cameras mounted to look directly downwards at the ground. This simplifies recognition as there
98 is no perspective, and all parts of the ground look the same. However this imposes physical
99 limitations on precision robots, which must either mount a camera physically outside the robot's
100 base footprint, or inside the body of the robot looking directly under its base. Much UK
101 grassland is found in less-favoured areas, including hilly and rocky terrain such as sheep farms.
102 These terrains often include obstacles which robots must navigate around, and such navigation
103 is complicated by physical extrusions beyond robot platform bases such as cameras on arms or
104 beams. Similarly, robots designed for these terrains may need heavy, protective bases which
105 prevent cameras or sprayers from being mounted directly downwards from them. To generalise
106 operation beyond flat grassland to cases such as these, it is more convenient and lower-cost to
107 use more standard camera mountings on top of the robot body, with cameras facing forwards
108 and tilted down, as in [2]. While this is a more robust physical solution, it makes the machine
109 vision problem harder as it must now deal with perspective. Further, the previous studies all
110 use clean images taken by stationary cameras to ease recognition. In practice, precision robots
111 operating in generalised terrains will be moving at speed, capturing images during motion. It is
112 not practical to stop every time an image must be taken. While camera stabilisation systems are
113 available at a cost, grassland and especially hill farmers typically require lower budget solutions
114 than arable farmers, so it is of interest to test algorithms on data collected from similar moving
115 robot platforms as would be used in practice, which can include motion blur.

116 Recent work has begun to explore the use of 3D lidar based sensing and detection of *Rumex*
117 in grassland [3, 29, 30]. While a similar independent evaluation of such data would also be of

118 interest, it is beyond the scope of the present machine vision study. Also beyond our scope
119 are non-visual approaches to weed detection including hyper-spectral [23, 24, 38], and chemical
120 sensing methods [26]. Our scope of detection of weeds in grassland is a particular sub-field of
121 automated weed detection in general, which has developed a wider range of methods applicable
122 to simpler cases of crops and weeds growing in flat, row-crop settings, which can typically
123 simplify the task by initial segmentation into green and brown discrete plant and soil regions,
124 unlike the grassland case where everything is green [7, 14, 21, 32, 36, 36].

125 1.2 Data and algorithm requirements

126 To make a fair and useful comparison between the different algorithm types proposed for UK,
127 less-favoured area grassland weed recognition, and to extend the robustness of previous studies,
128 the following requirements were taken into account. 1. Data should be clearly split into training
129 and test sets. 2. Only a single run should be allowed of each algorithm on the test set. 3. The
130 algorithms should be implemented and tested independently of their original proposers. 4.
131 testing should be on *Urtica* as well as *Rumex*. 5. Data should be collected from a moving,
132 robust platform, with cameras mounted on top of its body and pitched downwards from the
133 plane. 6. Data size should be in the order order of thousands of image windows. 7. Classification
134 should be performed on standard sized windows, including for morphological methods which
135 should be restricted to run on the same windows as feature-based methods. 8. Windows should
136 be of a suitable spatial size and resolution to enable precision spraying. 9. Data should be
137 collected over a representative variety of different days, illumination, and weather conditions.

138 Taken together, these requirements are more challenging than settings used in the previous
139 studies. An independent evaluation should not seek to ‘sell’ any one algorithm with high rates,
140 and should not shy away from reporting low accuracies when they occur. This helps to avoid
141 any publication bias [28] which may have acted as a filter on previous tests. Due to interactions
142 between the requirements and differences in data types, we do not re-implement algorithms
143 directly but instead use similar or closely related methods. This is required in particular for
144 the morphological approaches which do not transfer directly to window classification, such as
145 the use of watershed segmentation to represent region based methods previously run on whole
146 images. We test classifiers that are based on and inspired by the collection of previous studies

147 as a whole rather than directly re-implementing and competing between them.

148 **2 Methods**

149 The objective of the experiments is to report, to a statistically significant level, the classification
150 performance of various classification methods for grass vs weed detection, i.e two-way classifi-
151 cations representing spray/no-spray decisions for a general herbicide. In general this is distinct
152 from the problem of recognising individual weed species. A ‘classification method’ or ‘method’
153 means a combination of one feature type with one classifier type. Care must be taken to avoid
154 contamination of classifier training with any information from test data.

155 **2.1 Image acquisition and pre-processing**

156 Test plots of weeds in grass were constructed on a dairy grassland farm in South Yorkshire, UK.
157 Slabs of *Urtica* approximately 0.2m squared were extracted from working fields and transplanted
158 into a 3m squared trench (Figure 2a). This process was repeated for *Rumex*. Transplanting real
159 slabs from areas of the working farm ensures maximum realism and avoids problems of growing
160 the weeds artificially, which could lead to unrealistic soil backgrounds in images. In particular,
161 the transplanted slabs also contain grass, soil, rocks, and other surface features of the real work-
162 ing grassland farm, though only in 0.2m squared slabs which human transplanters considered to
163 be fully ‘sprayable’. To make this decision, the human transplanters were instructed to collect
164 only slabs which they would be happy to completely spray with a manual backpack sprayer if
165 they were being employed to manually destroy weeds. The weedy turfs were watered daily for
166 two weeks to allow the plants to stabilise before data collection. Plots were located in a region
167 of the farm that is in direct sunlight (not in shade) throughout the day.

168 Stereo pair images² were acquired in 1080HD from each plot using auto-focusing cameras³

²Only the mono, left camera images are used in this study. Stereo images were captured for use in future comparison studies and are also made available as part of the dataset.

³After evaluating several industrial and consumer cameras, a pilot experiment determined that the C920 is sufficient and lowest cost for our purpose, having sufficient depth of field to cover the region of interest, and default shutter speed sufficient to give sharp images when driving the robot at around 4km/h. This camera’s auto-focus is also useful as we operate on somewhat uneven terrain, sufficient to sometimes blur images with a static focus. The auto-focus explores and adjusts different settings of the focus and chooses the one which minimises the blur (maximises entropy) near the center of the image, before taking and saving the final image. 1080HD (=2megapixels) was used as we assume that real-time processing above this resolution is difficult with currently available on-board hardware. Manual inspection of the pilot images suggested that distortion from depth-of-field

169 (C920, www.logitech.com) mounted on a tracked robot as in fig. 1. The cameras were fixed
170 to the robot’s left side, facing out at right angle yaw to the direction of travel, and at $\pi/8$
171 radians (22.5 degrees) pitch down, to give a view over a roughly 1m square area of ground. The
172 robot drove in circles around the plots whilst capturing pictures, randomised between 0m and
173 1m from the edge of the plots (figure 2b). This guarantees an equal balance of lighting and
174 shadow angles in the data, because each drive around the plot contains images of the plot from
175 all ground angles. The size of the plots, robot, and camera positions were selected such that
176 the plot contents fill the images. This setup removes the need for manual annotation of weed
177 classes in images, as we are assured that every part of every image is full of a weed class. One
178 image was taken every second.

179 Image acquisition was arranged into epochs, where a single epoch consisted of making re-
180 peated revolutions of each plot for a period of ten minutes (yielding twenty minutes of weed
181 image acquisition from the two weed types together), followed by fifteen minutes of grass image
182 acquisition. The open grassland contained a mixture of grasses including *Lolium multiflorum*,
183 *Festuca pratensis*, *Phleum pratense*, and *Holcus lanatus* with some *Trifolium repens* (clover).
184 Approximately half of the epochs were acquired under overcast weather conditions, whilst the
185 other half was acquired under bright or sunny weather conditions. Data capture was staged
186 over four days, with 10 epochs in total captured at random times of day from sunrise to sunset
187 during May 2016. Images were inspected manually and a small portion ($< 0.1\%$) removed due
188 to recording problems. Approximately a third of a terabyte of usable image data was thus
189 acquired in total, to our knowledge this is the largest and most multi-conditioned data set of
190 its kind.

191 Images were pre-processed in three steps: colour calibration, perspective dewarping, and
192 windowing.

193 In colour calibration, images are transformed to compensate for variations due to lighting
194 and weather conditions. Colour calibration acts to colour-standardise images (to a certain
195 extent) to simplify classification. It was performed using a colour bar present in all images,
196 recorded as part the robot camera frames (Figure 3). The colour bar was composed of five
197 coloured squares (red, blue, yellow, white and green) using standard colours of paint. A single

and motion-blur effects were usually small compared to other factors such as perspective distortion. The camera also makes adjustments for lighting but we override these with our own colour normalisation as detailed below.

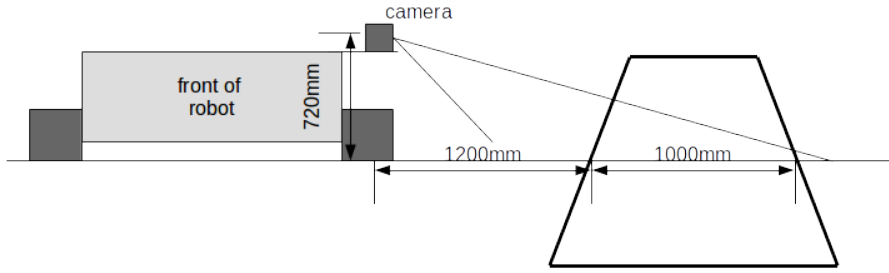


Figure 1: **Camera geometry.** Showing position of camera on tracked robot (viewed from the front), facing sideways. The thick black square shows the area on the ground, in perspective, used later in the perspective transform.



Figure 2: **Image acquisition.** a) Weed plot construction. b) Images were obtained using cameras mounted to the side of a tracked robot. The robot repeatedly made revolutions of each plot whilst taking pictures.

198 reference image was selected to calibrate all other images to. A measure of the blue, red and
 199 green light intensities from each coloured square on the bar was obtained as the mean value of
 200 the red, green and blue channels within the square. For each channel a vector of intensities was
 201 constructed with values for each coloured square, yielding the vectors \mathbf{b}_r , \mathbf{g}_r and \mathbf{r}_r for the blue,
 202 red and green channels, respectively. The subscript r indicates that these values are from the
 203 reference image. Repeating this procedure for a comparison image c (i.e. an image that is to
 204 be colour calibrated) gives vectors \mathbf{b}_c , \mathbf{g}_c and \mathbf{r}_c . A linear relationship between the intensities
 205 of the blue, red and green channels is assumed, measured from the reference image and the
 206 intensities of the blue, red and green channels measured from the comparison image. Given this
 207 assumption, the parameters for each channel, for example blue, are obtained as $\hat{\beta}(b)$,

$$\hat{\beta}(b) = (\mathbf{X}(b)^T \mathbf{X}(b))^{-1} \mathbf{X}(b)^T \mathbf{b}_c, \quad (1)$$

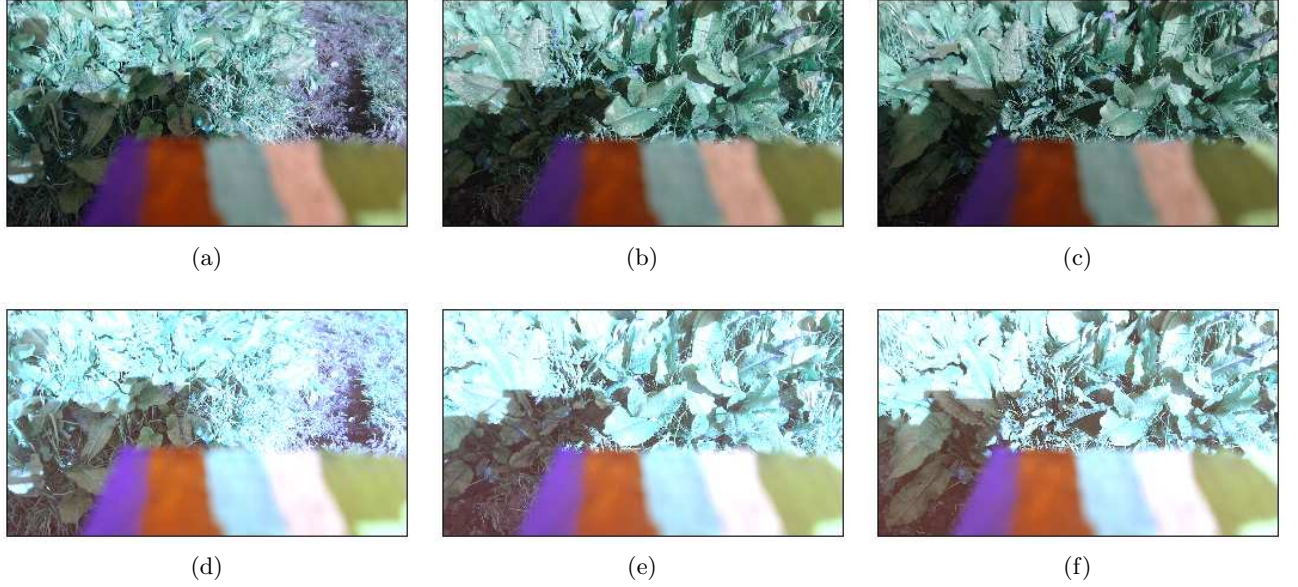


Figure 3: **Colour Calibration.** Figures a, b and c are raw images of dock leaves before any pre-processing has taken place. Figures d, e and f are colour calibrated versions of figures a, b and c, respectively.

208 where

$$\mathbf{X}(b) = \begin{pmatrix} \text{red}_r(b) & 1 \\ \text{blue}_r(b) & 1 \\ \vdots & \vdots \\ \text{green}_r(b) & 1 \end{pmatrix}, \mathbf{b}_c = \begin{pmatrix} \text{red}_c(b) \\ \text{blue}_c(b) \\ \vdots \\ \text{green}_c(b) \end{pmatrix}, \quad (2)$$

209 where the values in the left hand column of the matrix $\mathbf{X}(b)$ is the vector \mathbf{b}_r . These parameters
 210 are used to colour calibrate the blue channel of the comparison image as:

$$I'_c(b) = \frac{I_c(b) - \hat{\beta}(b)[1]}{\hat{\beta}(b)[2]}, \quad (3)$$

211 where the term in square brackets indexes a value in $\hat{\beta}(b)$, I is the original intensity and I' is
 212 the adjusted intensity. Performing these operations for the green and red channels also yields a
 213 fully colour calibrated image.

214 Perspective normalisation was performed via the projective transform shown in fig. 4a to
 215 those in fig. 4b. This maps a 1.16m width by 1.0m depth ground area into a 700 pixel width
 216 by 600 pixel height image, whose geometry is identical to that of a vertical, overhead camera
 217 as used in previous studies. However the image is not exactly the same as that of an overhead



Figure 4: **Perspective normalisation.** a) Raw image from left camera, with grid annotation showing 1.16m width x 1m depth on the ground. b) Affine transformation to remove perspective, grid annotation showing locations of the same rectangle after perspective transformation into a 600x700 pixel image.

218 camera due to the three dimensional structure of the plants. In particular, tall plants at the
 219 front of the image are inflated in size because they are warped as if they were further back.
 220 A key research question asks whether this will have a detrimental effect over pure overhead
 221 imaging.

222 Finally the dewarped image was split into regular 28×28 square or 64×64 square pixel win-
 223 dows for classification, corresponding to 46mm or 106mm squares of ground space respectively.
 224 Windows were contiguous and non-overlapping, and were stored for analysis. (These sizes were
 225 chosen to be around the scale of a single spray target radius, or ground size of a single weed or
 226 clump of weeds. 64 is a power of two which speeds up FFT based methods; 28 rather than 32 is
 227 chosen for the smaller window size to enable future comparisons with neural network methods,
 228 where 28^2 pixel windows are a common standard for historical and technical reasons [16].)

229 2.2 Dataset definitions

230 To avoid test data contaminating training processes, the set of epochs was first partitioned into
 231 training epochs and test epochs. This prevents, for example, classifiers from learning to recognise
 232 the lighting conditions rather than the weed types. Partitioning was performed manually to
 233 ensure a balance of weather conditions and weed types in each partition.

234 After partitioning the epochs, we defined training and hyper-training datasets by sampling
 235 random windows from the training epochs, and test and hyper-test data sets by random sampling

236 windows from the test epochs. (Separate hyper-training and hyper-test sets are used during
 237 hyper-parameter optimisation before training proper, to avoid contamination by test set data,
 238 as described in section 2.5.) A data set consisted of a set of images, where half of those were
 239 images of grass and the other half were images of weeds. A data set could contain an individual
 240 weed type (Rumex or Urtica) or a mixture of weed types (Rumex and Urtica). Similarly, a data
 241 set could contain images obtained under individual weather conditions (overcast or sunny) or a
 242 mixture of weather conditions (overcast and sunny). The data set sizes are shown in the table
 243 below,

244 Table 1: Dataset sizes.

Window size	Dataset type	Epoch set sampled	Number of windows
28 ²	Hyper-training	Training	10,000
28 ²	Hyper-test	Test	1,000
28 ²	Training	Training	200,000
28 ²	Test	Test	20,000
64 ²	Hyper-training	Training	2,000
64 ²	Hyper-test	Test	200
64 ²	Training	Training	40,000
64 ²	Test	Test	4,000

246 These sizes are still small compared with the total amount of raw data collected, but are
 247 orders of magnitude larger than data used in previous studies.

248 ⁴ The test set size was chosen to yield significant confidence in the results, while the training
 249 set size was selected to enable all the software implementations to train within one day of
 250 processing on a single 3GHz Intel core. Test and hyper-test datasets are 10% size of their
 251 corresponding training and hyper-training sets. The 28² sets are set to contain 5 times as many
 252 images as the 64² sets so that they contain the same amount of total pixel data ($28^2 \approx 64^2/5$),

⁴While the number of images is large, the number of actual plants imaged is smaller, because the many images are obtained by driving many times around the same plots of plants. However it is unlikely that images of the same plant are ever identical due to several factors. First, images were taken over several days, with collection days spaced several days apart. This allows the plants time to grow and move around between epochs. Second, within epochs, the plants are outdoor and exposed to wind, which moves their leaves constantly. Third, epochs are taken at different times of day, with different weather and light conditions. Fourth, the radius of the robot around the plots was randomised to +/-0.5m from the center line on each drive, ensuring different views. Fifth, the angles of the cameras shifted slightly between epochs during robot maintenance; this was deliberately not reduced, to introduce addition variation. Sixth, images were taken once per second, and it is unlikely that the robot would be at exactly the same angle around the plot at any two imaging moments. We assume that the additional variability from using more individual plants would be small compared to the variability introduced by these factors.

253 to allow results to be meaningfully compared across window sizes.

254 **2.3 Feature extraction**

255 The windowed images contain 64^2 or 28^2 pixels of RGB data, which are too large to use directly
256 as input vectors to most classifiers. Therefore, features were first computed from the data, as
257 in the previous studies. The selection of features used is detailed below and was selected to
258 represent most previously proposed feature choices. All features ran on greyscale versions of
259 the windows (obtained as the mean of the RGB channels), which is justified as all images are
260 primarily all the same shade of green (unlike the case in detection studies of arable crop weeds
261 in brown soil).

262 **2.3.1 Fourier Transform**

263 The Fourier Transform [39] represents an image in the basis of its orthogonal harmonic frequency
264 components. For digital images the discrete Fourier transform (DFT) is used, whose basis is a
265 set of two dimensional harmonics large enough to fully describe the spatial domain image. The
266 number of frequencies corresponds to the number of pixels in the spatial domain image. For a
267 square image of size $N \times N$, the two-dimensional DFT is given by:

$$F(k, l) = \sum_{i=0}^{N-1} \sum_{j=0}^{N-1} f(i, j) e^{-i2\pi(\frac{ki}{N} + \frac{lj}{N})}, \quad (4)$$

268 where $f(i, j)$ is the image in the spatial domain and the exponential term is the basis function
269 corresponding to each point $F(k, l)$ in the Fourier space. The basis functions are two dimensional
270 sinusoidal waves of increasing spatial frequencies, i.e. $F(0, 0)$ represents the DC-component of
271 the image which corresponds to the average brightness and $F(N - 1, N - 1)$ represents the
272 highest frequency. The absolute values of the DFT yield the image's magnitude of frequency
273 spectrum which is used as the feature vector for classification. We denote this method of feature
274 extraction as FT. The Fourier transform is illustrated in figure 5, which shows that broad leaves
275 tend to contain stronger low spatial frequencies while grass' thin blades give rise to higher spatial
276 frequencies.

277 **2.3.2 Local binary patterns**

278 Local binary patterns (LBP) are a texture description feature [15]. Local means they are
279 computed on local sub-windows of an image only, as a function of a center pixel and either its
280 immediate or r pixel radius neighbours; binary means that the feature vector is binary, with
281 each feature classed as either present or absent. Windows are converted to greyscale, then for
282 each pixel $x_{i,j}$ in the window, LBP computes an 8-element binary vector,

$$283 \quad [(x_{i,j} > x_{i,j+r}), (x_{i,j} > x_{i-r,j+r}), (x_{i,j} > x_{i-r,j}), (x_{i,j} > x_{i-r,j-r}), (x_{i,j} > x_{i,j-r}), (x_{i,j} > \\ 284 \quad x_{i+r,j-r}), (x_{i+r,j} > x_{i,j}), (x_{i,j} > x_{i+r,j+r})].$$

285 There are $2^8 = 256$ possible values of this feature vector, with oriented edge and corner
286 detection present as special cases. LBP computes feature vector for each pixel in the window,
287 then computes a 256-point histogram of the obtained values over the window. The shapes of
288 these histograms are considered to be characteristic of the texture classes and are given as input
289 to classifiers. As well as using the eight near neighbours as above, a hyper-parameter n_{points}
290 can also be used to generalise to other numbers of quantised comparison points equally spaced
291 on a circle around the center. (Many other variations on the LBP concept have also been
292 proposed [13] but are beyond the scope of the present comparison study.)

293 **2.3.3 Interest points and k-means**

294 The above features treat every pixel in the window as equally important, and are considered to
295 represent texture-like properties. An alternative approach is to locate only ‘interesting’ points
296 within the window and base classification on these. In particular, weeds such as *Urtica* have
297 many distinctive jagged corners which might form useful points on which to base classification.
298 Interest point method contain two feature extraction steps prior to classification. First, interest
299 points are located; second, the local region at each of these points is used to extract a feature
300 descriptor. Points are considered interesting if they contain a mixture of colours and can be
301 uniquely located, i.e. a corner is interesting because there is only one location where it exists,
302 while an edge is less interesting because it exists along a line of locations. Feature classes used to
303 describe these points are usually wavelet-like, combining color, frequency and size information.

304 Precise definition of useful interest point detectors and descriptors normalising these prop-

305 erties has been and remains an active area of machine vision research [25], but the present study
 306 arbitrarily selects the state-of-the-art Scale-Invariant Center-Surround Detectors (CenSurE) [1]
 307 interest point detector and the Binary Robust Invariant Scalable Keypoints (BRISK) [20] de-
 308 scriptor to represent the general class of methods. CenSurE finds an approximation to the set
 309 of corner-like points defined by,

$$\{\lambda_d(H(x)_{i,j}) > t, d \in \{1, 2\}\}, \quad (5)$$

310 where λ_d are the two eigenvalues of the Hessian matrix H of the image x at each pixel i, j , and
 311 t is a threshold. Both eigenvalues are maximal at corners of any rotation. Rather than compute
 312 this computationally intensive (due to eigenvalue finding) test for every pixel, CenSurE first
 313 performs a faster pre-screening step, using a set of scaled filters to approximate the Laplacian
 314 (total curvature) at each pixel, then only computing the Hessian test at local maxima of this
 315 curvature [1].

316 BRISK descriptors are similar to the LBP vectors above, but using pixel intensity compar-
 317 isons,

$$f_n = (x_{i,j} > x_{i'_n, j'_n}), \quad (6)$$

318 at a larger set of 256 offsets $\{a_n, b_n\}$ giving $(i'_n = i + a_n, j'_n = j + b_n)$. Unlike LBP, these offsets
 319 are not equally spaced around a circle, but may form any arbitrary pattern. Together with the
 320 larger number of points, this may capture potentially higher-order information than in LBP.
 321 Standard values of the offset patterns are used as provided in [20].

322 When BRISK feature vectors have been computed for all images in the training set they are
 323 passed to the k -means algorithm which clusters them into K regions in feature space, where
 324 feature space is a finite p -dimensional vector space with each dimension representing a BRISK
 325 feature of an image. Initiating K random clusters we firstly calculate the Euclidean distance
 326 between the i th BRISK vector \mathbf{x}_i and the k th cluster \mathbf{C}_k

$$d_{i,k} = \left[\sum_{j=1}^p (\mathbf{x}_{ij} - \mathbf{C}_{kj})^2 \right]^{1/2}. \quad (7)$$

327 After performing this operation for all clusters we can then assign the BRISK vector to the

328 cluster that minimises d (Equation 7). This operation is then performed for each BRISK
 329 vector. Knowing the members of each group we can now compute the new centroid of each
 330 group based on these new memberships. New centroids are the average coordinates among new
 331 members,

$$\mathbf{C}_k = \frac{\sum_{n=1}^{N_k} \mathbf{X}_{n1}}{N_k}, \dots, \frac{\sum_{n=1}^{N_k} \mathbf{X}_{np}}{N_k}, \quad (8)$$

332 where N_k is the number of BRISK vectors in cluster k . This whole process is then repeated until
 333 the BRISK vectors cease to move groups (i.e. until the computation of the k-means clustering
 334 has reached stability).

335 Clustering observed BRISK vectors in this way defines K discrete types of BRISK feature.
 336 For any given image, we may now extract each of its interest points, compute a BRISK descriptor
 337 at these points, then replace each of their BRISK descriptors with one of these quantised types.
 338 This allows us to then count how many c_k of each discrete BRISK types $k = 1 : K$ appear in
 339 the image. The vector of these counts, $\{c_k\}_{k=1:K}$ is then used as a feature descriptor of the
 340 whole image.

341 We refer to this feature as $B > K$, (for ‘BRISK followed by k -means’).

342 2.3.4 Watershed segmentation

343 We wish to test window-based features against region-growing type methods as proposed in
 344 previous studies. To make a fair comparison it is necessary to substitute pure region growing
 345 with a similar but window-based method. Otherwise the region growing methods could be
 346 accused of accessing more data to make classifications of each region, from the whole image,
 347 rather than just from its local window. For this purpose, we use a watershed method as a close
 348 substitute. Watershed segmentation [37] was originally developed for the purpose of separating
 349 touching objects in an image rather than for classification, but may also be used as a region-
 350 growing type classifier. The watershed transform finds ‘catchment basins’ and ‘watershed ridge
 351 lines’ in an image by treating it as a surface where light pixels are high and dark pixels are low.
 352 Segmentation using the watershed transform works better if a human operator can first identify,
 353 or ‘mark’, pixels from foreground objects and background locations. The marker-controlled
 354 watershed segmentation used in the present study follows a multi-step procedure.

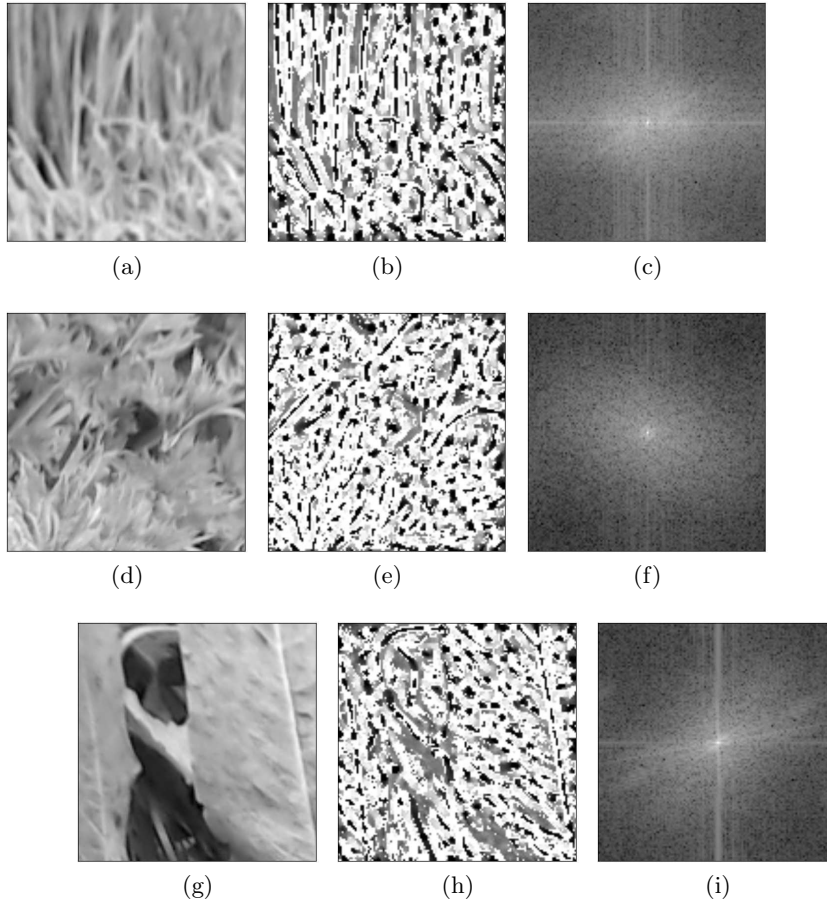


Figure 5: **Feature extraction.** Figures a, d and g are fully pre-processed images containing grass, Urtica and Rumex leaves, respectively. Figures b, e and h are the local binary patterns (LBPs) of images a, d and g, respectively (with $n = 24$, $r = 4$). Figures c, f and i are the magnitude of frequency spectra of images a, d and g, respectively.

355 Given a grey-scale image as input, we apply Otsu’s thresholding [37] to segment the back-
356 ground from the foreground. Then we compute the Euclidean distance transform which com-
357 putes the Euclidean distance to the closest zero (i.e. background pixel) for each of the foreground
358 pixels. Doing this yields the distance map d . Next we apply a function $f(d, d_{\min})$ that finds the
359 peaks (local maxima) in the distance map, and ensures that we have at least a d_{\min} pixel dis-
360 tance between each peak. Then we apply a connected component analysis using 8-connectivity
361 to the output of f , the output of which gives us our markers, which we then feed in to the
362 watershed function. The watershed function returns a matrix of labels, an array with the same
363 width and height as the input image. Each pixel value has a unique label value. Pixels that
364 have the same label belong to the same object. For a given image, we then count the number
365 of *unique* labels or *segments*. Performing these operations for multiple values of d_{\min} yields

366 multiple counts of segments for a given image, and thus a feature vector for classification. We
367 denote this method of feature extraction as W .

368 2.4 Classifiers

369 The following classifiers were used to represent previously proposed architectures. Each classifier
370 (SVM, LDA, NN) can take as its input any feature type obtained from windows (LBP, FT, B)K,
371 W). This yields 12 distinct classification methods, LBP)SVM, FT)SVM, B)K)SVM, W)SVM,
372 LBP)LDA, FT)LDA, B)K)LDA, W)LDA, LBP)NN, FT)NN, B)K)NN and W)NN. For example,
373 LBP)SVM means that we pass the local binary pattern feature vector as input to a support
374 vector machine, whilst FT)LDA means that we pass the image’s frequency spectrum magnitude
375 feature vector as input to linear discriminant analysis.

376 2.4.1 Support Vector Machines

377 A Support Vector Machine [35] models the a classification problem as finding a non-linear
378 partition of the feature vector space into classes (e.g. grass or weeds), formed as a linear
379 partition of a higher-dimension space formed by non-linear high-dimensional projection of the
380 feature vectors. To understand how SVMs work it is useful to first briefly describe the support
381 vector classifier (SVC). The SVC separates images into their classes by finding the *linear affine*
382 hyper-plane that maximises the distance (known as the margin M) between the two image
383 classes in feature space. Observations that fall on the boundaries of the margin are the support
384 vectors.

385 The linear affine hyper-plane is defined by the following inner product,

$$\mathbf{b} \cdot \mathbf{x} + b_0 = 0, b_0 \neq 0, \tag{9}$$

386 where \mathbf{x} is a p -dimensional training image feature vector with associated weights \mathbf{b} . Now
387 consider a set of n p -dimensional training image feature vectors, \mathbf{x}_i , each with an associated
388 class label $y_i \in \{-1, 1\}$. Introducing new hyper-parameters; n ϵ_i values (known as slack values)
389 and a hyper-parameter C (known as the budget), then we wish to maximise M across b_1, \dots, b_p ,

390 $\epsilon_1, \dots, \epsilon_n$ such that

$$\sum_{j=1}^p b_j^2 = 1, \quad (10)$$

391 $y_i(\mathbf{b} \cdot \mathbf{x} + b_0) \geq M(1 - \epsilon_i), \forall_i = 1, \dots, n,$ (11)

392 $\epsilon \geq 0, \sum_{i=1}^n \epsilon_i \leq C,$ (12)

393 where C , the budget, is a non-negative ‘tuning’ hyper-parameter and hyper-parameters ϵ_i allow
394 the individual observations (i.e. training images) to be on the wrong side of the margin or
395 hyper-plane. C collectively controls how much the individual ϵ_i can be modified to violate the
396 margin.

397 SVMs are an extension of SVCs that results from a non-linear enlargement of the feature
398 space through the use of functions known as kernels. This enlargement of the feature space
399 means that observations from different classes can be separated in many more ways than they
400 could be otherwise. To obtain the SVM, firstly we note that it is possible to show that a linear
401 support vector classifier for a particular observation can be represented as a linear combination
402 of inner products for the subset ℓ of training observations that represent the support vectors,

$$f(\mathbf{x}) = b_0 + \sum_{i \in \ell} \alpha_i \langle \mathbf{x}, \mathbf{x}_i \rangle, \quad (13)$$

403 where α_i are the coefficients. Replacing the inner product $\langle \mathbf{x}_i, \mathbf{x}_k \rangle$ with a more general inner
404 product ‘kernel’ function $K = K(\mathbf{x}_i, \mathbf{x}_k)$, we can modify the SVC representation to use non-
405 linear kernel functions. One example is the radial (RBF) kernel,

$$K(\mathbf{x}_i, \mathbf{x}_k) = \exp \left(-\gamma \sum_j^p (\mathbf{x}_{ij} - \mathbf{x}_{kj})^2 \right), \gamma > 0. \quad (14)$$

406 Intuitively, the γ parameter defines how far the influence of a single training example reaches,
407 with low values meaning ‘far’ and high values meaning ‘close’. The γ parameter can be seen as
408 the inverse of the radius of influence of samples selected by the model as support vectors.

409 The algorithmic solution for the SVM is one that finds optimal values for the coefficients α
410 and the slack variables ϵ_i . Typically gradient decent algorithms are used. The hyper-parameters
411 C and γ are set/optimised by the user.

412 Finally, a test image is classified according to whether its feature vector \mathbf{x}^* results in a
 413 positive or negative sign when passed into the function $f(\mathbf{x}^*)$. Note that feature vectors were
 414 normalised before being passed into the support vector machine. We denote this classifier as
 415 SVM.

416 2.4.2 Linear Discriminant Analysis

417 As with SVCs/SVMs, Linear Discriminant Analysis [22] models the classification problem by
 418 creating a feature space with a dimension for each feature. However, in LDA, observations from
 419 2 separate classes are assumed to be sampled from 2 separate multivariate Gaussian distributions
 420 in feature space with different means but the same covariance matrix. Given those assumptions
 421 we have a linear hyperplane perfectly separating the means of the 2 distributions. This means
 422 that any observation that is situated above the hyperplane has a higher probability of being a
 423 sample from the Gaussian whose mean is situated above the hyperplane than being a sample
 424 from the Gaussian whose mean is located below the hyperplane.

425 To explain LDA in some more detail, firstly we write Bayes' rule for the classification prob-
 426 lem

$$P(i|\mathbf{x}) = \frac{P(\mathbf{x}|i)P(i)}{\sum_j P(\mathbf{x}|j)P(j)}, \quad (15)$$

427 where the likelihood function $P(\mathbf{x}|i)$ gives the probability that the observation \mathbf{x} is a sample
 428 from the Gaussian representing the class i and $P(i)$ is the prior probability of the class i . From
 429 Bayes' rule and the assumptions outlined we can derive the linear discriminant analysis formula

$$f_i = \mathbf{m}_i \mathbf{C}^{-1} \mathbf{x}_k^T - \frac{1}{2} \mathbf{m}_i \mathbf{C}^{-1} \mathbf{m}_i^T + \log(p_i), \quad (16)$$

430 where \mathbf{m}_i is a vector containing the mean of each feature for the class i and \mathbf{C} is the pooled
 431 within group covariance matrix which is a weighted mean of the covariance matrix \mathbf{C}_i for each
 432 class. For a total of n observations, N classes and n_i observations in each class \mathbf{C} is

$$\mathbf{C} = \frac{1}{n} \sum_{i=1}^N n_i \mathbf{C}_i. \quad (17)$$

433 Then we simply assign a test image k to group i that has maximum f_i . We denote this classifier

434 as LDA.

435 **2.4.3 ‘Nearest Neighbour’ Classifier**

436 Nearest neighbour is a very simple classifier, used here to provide a baseline to compare with
437 the two more sophisticated classifiers (SVM and LDA) above. In its training phase, the nearest
438 neighbour classifier computes the median feature vector for each class (grass or weeds). A test
439 image is then classed as grass if its feature vector minimises the sum of absolute errors between
440 it and the median feature vector computed from grass images. Likewise a test image is classed
441 as containing weeds if its feature vector minimises the sum of absolute errors between it and
442 the median feature vector computed from images containing weeds. We denote this classifier as
443 NN.

444 **2.5 Hyper-parameter optimisation**

445 Some of the classifiers and features have hyper-parameters which define how training is com-
446 puted. Previous studies have mostly reported the best obtained results of methods on test sets,
447 and stated the hyper-parameter values used to give them. However it is unclear whether the
448 hyper-parameters in these cases have been set in advance of the evaluation on the test sets, or
449 if they have been fit to the test data by running method multiple times on the test data and
450 reporting only the best result.

451 To avoid this potential bias, careful use was made of hyper-training and hyper-test datasets,
452 independent of both training and test datasets, to select hyper-parameters in advance of the
453 main training and test phases. Hyper-parameters were optimised on these sets, so that each
454 system only saw the final test set only once for its reportable evaluation score.

455 In theory, hyper-training could be performed by training many versions of a classifier on the
456 full training dataset, then scoring them against a hyper-test set, and selecting the best performer.
457 (The hyper-test sets are sometimes known as ‘validation sets’). However this requires running
458 time-consuming training many times. So given the large ratio of data to compute resources
459 available for this study, a smaller hyper-training dataset, of 5% size of the full training dataset,
460 was used in place of the training dataset. This greatly reduces the required computation time
461 but was found to still give a reasonable indication of good hyper parameters to use within

462 available compute resources.

463 SVMs have two hyper-parameters (C and γ) that should be optimised. We set C and γ
464 in exponentially growing sequences, $C = 2^{-5}, 2^{-3}, \dots, 2^{15}$, $\gamma = 2^{-15}, 2^{-13}, \dots, 2^3$, which has been
465 shown to be a practical method for identifying good parameters [19]. In addition the parameters
466 (number of points n_{points} and radius r) of the LBP should also be optimised. For all experiments
467 we set $n_{\text{points}} = 2, 4, \dots, 30$. For experiments with 28^2 pixel windows we set $r = 1, 2, \dots, 8$ while
468 for experiments with 64^2 pixel windows we set $r = 2, 4, \dots, 16$ (r has maximum value equal to a
469 quarter of the image width). For all experiments involving the B)K method of feature extraction
470 we optimised K for values $K = 1, \dots, 28$. For all experiments involving the W method of feature
471 extraction we optimised the minimum distance term d_{min} in growing sequences of integers
472 $[1], [1, 2], \dots, [1, \dots, 15]$. For the sequence $[1, 2]$, for example, we would generate a feature vector
473 by first setting $d_{\text{min}} = 1$, passing an image into the W method and retrieving the number of
474 segments. Then the process would be repeated for $d_{\text{min}} = 2$ and both segment values would be
475 appended, yielding a feature vector of length 2. Thus the length of a particular sequence is the
476 length of the feature vector generated by the W method of feature extraction.

477 In addition to numerical hyper-parameters, SVMs can further use various kernels and LDA
478 can further use various types of ‘solver’ and both SVMs and LDA have an option to apply a
479 ‘shrinking’/‘shrinkage’ heuristic. For the LBP)SVM method we reduced the number of param-
480 eter permutations to consider by assuming some independence between parameters. Thus we
481 first optimised C and γ , (considering all permutations of C, γ) for a fixed $n_{\text{points}} = 15, r = 4$
482 for 28^2 pixel windows and a fixed $n_{\text{points}} = 15, r = 8$ for 64^2 pixel windows, for each kernel with
483 the shrinking heuristic turned on and off. Then we fixed C, γ and the kernel at their optimal
484 values and optimised n_{points} and r (considering all permutations of n_{points}, r). For all other
485 classification methods we considered all possible parameter permutations.

486 LDA’s r and BRISK’s CenSurE approximation variables were also treated as hyper-parameters.
487 Details of the results on the hyper-test set from hyper-training that are used to set hyper-
488 parameters for full training are shown in the Appendix.

489 2.6 Experiments

490 After hyper-parameter optimisation, we evaluated the performance of each feature-classifier
491 combination by training from scratch on the full training dataset and testing for the first and
492 only time on the test dataset.

493 To enable a fair comparison of systems running on the two different window sizes, more
494 windows were present in the 28^2 pixel training and test sets than in the 64^2 pixel sets. This is
495 because each 64 pixel image contains roughly five times as much visual information as each 28
496 pixel image ($28^2/64^2 = 0.19$); each 64^2 pixel image is effectively five 28^2 pixel windows joined
497 together. Therefore, in the 28^2 pixel case, we used a training set of 200,000 windows and a test
498 set of 20,000 windows, each comprised of half grass and half weed windows; while in the 64^2
499 pixel case we used 1/5 as many windows: 40,000 training and 4,000 test, also comprised of half
500 grass and half weeds.

501 The most important practical question for weeding robots is the performance in mixed weeds
502 (Rumex+Urtica) and in mixed weather (sunny+overcast), for the two window sizes. Window
503 size is important because it controls the spatial resolution at which the robot could spray the
504 weeds – in square windows of 106mm or 56mm. As the key research question, performance was
505 evaluated for every one of the twelve feature-classifier combinations on both window sizes.

506 It is sometimes the case in machine learning that improved accuracies can be obtained by
507 fusion results from multiple methods into *meta-classifiers* (also known as ensemble learning).
508 Many combination algorithms are available with different and subtle assumptions which are still
509 sometimes debated [8, 9].⁵ To give a simple illustrative, though non-optimal, idea of what per-
510 formance improvements could be available, three simple, standard fusion methods were tested.
511 First, a simple voting scheme, META-VOTE, assigns an equal weight to each classifier’s output,
512 and yields the classification with the most votes. (In the case of a tie, the best classifier’s output
513 is given the deciding vote.) Second, META-ACC weights the votes of each classifier by its ac-
514 curacy. Finally, META-LDA considers the output of each classifier as an element of a Boolean

⁵Until recently it was often assumed that optimal combination could be achieved via Bayesian Model Averaging (BMA), which makes class predictions c of input x from models M_i and training data D as $P(c, x) = \sum_i P(c|M_i, x)P(M_i|D)$. However it is now known that for large data sets, BMA simply converges to the outputs of the single best classifier in the ensemble, ignoring the others [9], hence it is not used here. This problem with BMA is caused by its underlying assumption that the ensemble contains the perfect, ground-truth model rather than just a set of approximations.

515 feature, and trains a new LDA classifier to predict ground truth class from these vectors.⁶

516 Secondary questions of interest include the effects of perspective, weather type, weed type,
517 and windowing. As a full training process can take several days, these questions were examined
518 using only the best feature+classifier system and assumed to be independent of one another.

519 To examine the effect of perspective unwarping, the test set (containing grass under mixed
520 weather conditions, and mixed weeds under mixed weather conditions), was split into new test
521 sets according to their windows' vertical locations (row numbers) in the camera images for indi-
522 vidual scoring. Low row numbers indicate windows from the base of the image, corresponding
523 to space close to the robot cameras, while high row numbers indicate windows at the top of the
524 image, from space furthest from the robot cameras.

525 To examine the effect of weather, each epoch was classified as sunny or overcast, and the
526 original test set was split into two test sets comprised of windows of these weather types for
527 individual evaluation.

528 To examine the effect of weed type on classifier performance, two set sets were created which
529 contained only grass-and-Urtica and grass-and-Rumex respectively, for individual evaluation.

530 To give an idea of performance in the limiting case of large windows full of weeds or grass,
531 we assessed the performance of the B)K)SVM classification method on full sized (600×700)
532 pixel windows from data sets containing grass vs mixed and individual weed types under mixed
533 weather conditions. We conducted this experiment because BRISK features are more usually
534 extracted from full-view images than from the standardised windows used in the rest of this
535 study. Thus we wished to asses the performance of this particular classification method under
536 its own ideal conditions. As with other experiments, hyper-parameters were optimised on
537 hyper-training and hyper-test datasets (though of new 600×700 windows and set sizes hyper-
538 training=1000, hyper-test=200, training=10,000,test=2000 , before training and testing on the
539 training and test datasets.

⁶To estimate META-LDA performance on new data without corruption by training the meta-classifier on test data, the test set was split into two random partitions with one used to train the new LDA and the other to test it. This means the result quoted from only a subset of the original test set. However the original and partitioned test sets are sufficiently large to maintain tight Bayesian confidence internals in the accuracy posteriors to be comparable with the other results.

Table 2: Results of applying all 12 classification methods to 28^2 pixel window test dataset containing grass vs mixed weeds, mixed weather, after training on 28^2 pixel window training dataset. *ACC* is over all accuracy, i.e. the probability that a random image is correctly classified. *CI* is the confidence interval in the estimate of *ACC*. *GRASS* and *WEED* are probabilities that images of grass, or weed, respectively, are correctly classified. ‘NA’ stands for ‘Not Applicable’, ‘shk’ for ‘shrinking’.

540

541

METHOD	ACC	CI	GRASS	WEED	PARAMETERS
LBP)SVM	68.75	3.27×10^{-3}	74.1	63.6	$n_{\text{points}} = 20, r = 5, \text{kernel}=\text{RBF}(\text{shk}), C = 2^{13}, \gamma = 2^{-1}$
B)K)SVM	52.70	3.53×10^{-3}	38.8	67.1	$K = 4, \text{kernel}=\text{linear}(\text{shk}), C = 2^{-5}$
FT)SVM	71.80	3.18×10^{-3}	79.0	64.7	$\text{kernel}=\text{RBF}(\text{shk}), C = 2^1, \gamma = 2^3$
W)SVM	64.67	3.38×10^{-3}	72.1	57.1	$d_{\text{min}} = [1, \dots, 11], \text{kernel}=\text{RBF}(\text{shk}), C = 2^{15}, \gamma = 2^{-3}$
LBP)LDA	65.25	3.37×10^{-3}	71.1	59.1	$n_{\text{points}} = 28, r = 3, \text{solver}=\text{svd}$
B)K)LDA	53.97	3.52×10^{-3}	63.6	44.1	$K = 20, \text{solver}=\text{lsqr}(\text{shh})$
FT)LDA	68.54	3.28×10^{-3}	78.9	63.2	$\text{solver}=\text{lsqr}(\text{shk})$
W)LDA	61.63	3.44×10^{-3}	69.4	53.8	$d_{\text{min}} = [1, \dots, 5], \text{solver}=\text{lsqr}(\text{shk})$
LBP)NN	62.93	3.41×10^{-3}	69.6	66.3	$n_{\text{points}} = 2, r = 4$
B)K)NN	50.00	3.54×10^{-3}	0.0	100.0	$K = 17$
FT)NN	61.79	3.44×10^{-3}	62.3	60.8	NA
W)NN	65.77	3.35×10^{-3}	65.6	66.1	$d_{\text{min}} = [1, \dots, 10]$
META-VOTE	71.38	3.20×10^{-3}	76.5	66.3	NA
META-ACC	71.90	3.18×10^{-3}	76.5	67.3	NA
META-LDA	73.47	4.41×10^{-3}	75.8	71.1	NA

542

Table 3: Results of applying all 12 classification methods to 64^2 pixel window test dataset containing grass vs mixed weeds, mixed weather, after training on 64^2 pixel window training dataset. *ACC* is over all accuracy, ie. the probability that a random image is correctly classified. *CI* is the confidence interval in the estimate of *ACC*. *GRASS* and *WEED* are probabilities that images of grass, or weed, respectively, are correctly classified. ‘NA’ stands for ‘Not Applicable’, ‘shk’ for ‘shrinking’.

543

544

METHOD	ACC	CI	GRASS	WEED	PARAMETERS
LBP)SVM	82.88	5.96×10^{-3}	87.1	78.7	$n_{\text{points}} = 24, r = 4, \text{kernel}=\text{RBF}(\text{shk}), C = 2^9, \gamma = 2^3$
B)K)SVM	69.15	7.27×10^{-3}	70.4	69.0	$K = 17, \text{kernel}=\text{RBF}, C = 2^1, \gamma = 2^8$
FT)SVM	79.40	6.39×10^{-3}	84.6	74.2	$\text{kernel}=\text{RBF}(\text{shk}), C = 2^3, \gamma = 2^1$
W)SVM	73.23	7.00×10^{-3}	79.0	67.5	$d_{\text{min}} = [1, \dots, 10], \text{kernel}=\text{RBF}(\text{shk}), C = 2^{11}, \gamma = 2^3$
LBP)LDA	75.50	6.80×10^{-3}	82.3	68.7	$n_{\text{points}} = 16, r = 4, \text{solver}=\text{lsqr}(\text{shk})$
B)K)LDA	70.65	7.16×10^{-3}	81.6	60.9	$K = 17, \text{solver}=\text{lsqr}(\text{shk})$
FT)LDA	73.15	7.01×10^{-3}	82.6	63.7	$\text{solver}=\text{eigen}(\text{shk})$
W)LDA	63.13	7.63×10^{-3}	88.1	38.2	$d_{\text{min}} = [1, \dots, 15], \text{solver}=\text{svd}$
LBP)NN	72.43	7.06×10^{-3}	77.0	68.0	$n_{\text{points}} = 10, r = 12$
B)K)NN	70.55	7.40×10^{-3}	71.5	63.7	$K = 18$
FT)NN	63.08	7.63×10^{-3}	58.7	67.5	NA
W)NN	74.48	6.89×10^{-3}	76.0	73.1	$d_{\text{min}} = [1, \dots, 5]$
META-VOTE	78.63	6.48×10^{-3}	89.4	67.9	NA
META-ACC	80.90	6.21×10^{-3}	88.4	73.8	NA
META-LDA	83.40	8.42×10^{-3}	i84.9	81.9	NA

545

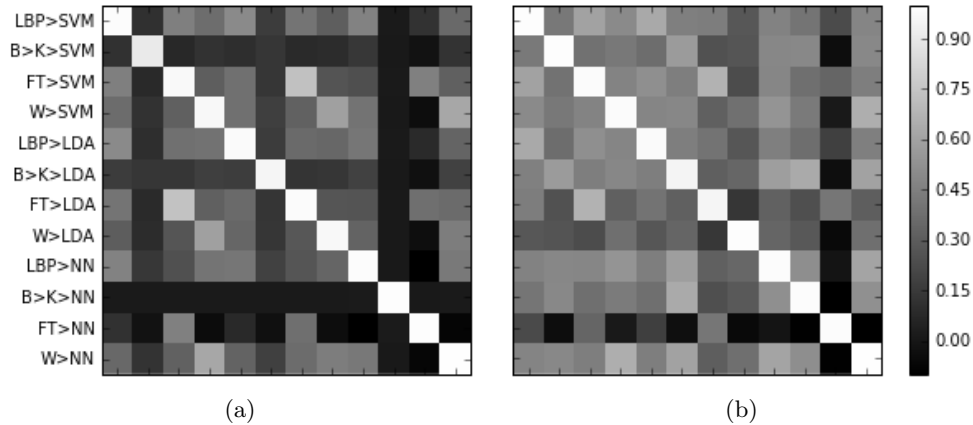


Figure 6: **Covariance Matrices.** a) Covariance between the 12 classification methods when applied to 28 pixel squared windows (grass vs mixed weeds, mixed weather). b) Covariance between the 12 classification methods when applied to 64 pixel squared windows (grass vs mixed weeds, mixed weather).

546 3 Results

547 Tables 2 and 3 give the results for training and testing the 12 classification methods on 28^2 and
 548 64^2 pixel windows, respectively, both with mixed weather and mixed weed types. *ACC* shows
 549 the overall accuracy of each method, as the proportion of images correctly classified. Bayesian
 550 confidence intervals (CI) computed as standard deviations of the Beta distribution posteriors
 551 over belief in the accuracy [5], assuming flat priors, are also given for each classification method,
 552 which justify the significance of the accuracy percentages to two decimal places. (We also list
 553 breakdown accuracies for grass and weed image presentations, which indicate rates of false
 554 positive and false negatives.) These experiments were conducted to determine which classifier
 555 was the most accurate in predicting test images from data sets containing mixed weeds and
 556 mixed weather conditions.

557 The LBP>SVM method performed better than the other classification methods for experiments
 558 using 64^2 pixel windows, with an accuracy of 82.88%. This was achieved with the SVM kernel
 559 set to RBF with the shrinking heuristic turned on, the hyper-parameters of the LBP set to
 560 $n_{\text{points}} = 24$, $r = 4$ and the hyper-parameters of the SVM set to $C = 2^9$, $\gamma = 2^3$. The FT>SVM
 561 method performed better than the other classification methods for experiments using 28^2 pixel
 562 windows, with an accuracy of 71.80%. This was achieved with the SVM kernel set to RBF with
 563 the shrinking heuristic turned on, and the SVM hyper-parameters set to $C = 2^1$, $\gamma = 2^3$.

564 The META-VOTE meta-classifier yielded worse results than the single best method in both

565 28^2 and 64^2 pixel windowed cases. This may be due to averaging of the best method with the
566 less good methods dragging down the overall result. This typically occurs when all or most
567 classifiers are acting on the same inherent information in the data but with different accuracies,
568 rather than acting on different types of information per method. Similarly, META-ACC gives
569 on a tiny improvement over the best method for 28^2 windows (71.90 vs 71.80), and is worse
570 than the best 64^2 pixel method (80.90 vs 82.88). META-LDA is the best of the meta-classifiers,
571 and is the only one to give significant improvements in both the 28^2 pixel (73.74 vs 71.80)
572 and 64^2 pixel (83.40 vs 82.88). (Significance can be seen by comparing the small CIs with the
573 larger accuracy differences). META-LDA's weights are more principled, and optimal under its
574 assumptions, than the heuristic META-VOTE and META-ACC, so its better performance is
575 expected. However the gain from using META-LDA over using just the single best method, in
576 each window case, is small. Again, this suggested that all the methods are operating on similar
577 information within the images rather than with different information. Further insight into this
578 possibility is gained by examining the correlation matrix of the 12 methods' predictions in fig.
579 6. Here, each grass/weed classification in the test set is considered to have a value of 0 or 1 for
580 grass/weed, and correlations over the test data are presented. It can be seen that the methods
581 are less correlated with one another in the 28^2 pixel case than in the 64^2 pixel case, which
582 explains why meta-classification works better for 28^2 than 64^2 windows. There are stronger
583 correlations between methods sharing the same feature type than methods sharing the same
584 classifier type, as can be seen by the secondary diagonal patterns. The FT>NN method has a
585 low correlation with the others because it is a very poor accuracy method.

586 Results for the distance experiment are shown in Figure 7a. The best performing feature-
587 classifier combination - the LBP>SVM method - is here run again on mixed weed and weather
588 test sets, separated as a function of the distance of the window from the robot camera's ground
589 location (for both 28^2 and 64^2 pixel-squared windows). Classification performance decreased
590 smoothly as the distance increased, for both 28^2 and 64^2 pixel windows, by a considerable
591 amount (by around 15% absolute for 64^2 windows, and 10% absolute for 28^2 windows.) Weeds
592 closest to the cameras were predicted with a 87.85% accuracy (for 64^2 pixel windows), which
593 is more in line with the high accuracies reported by the previous studies than with accuracies
594 at far distances. It should also be noted that this result was obtained for a mixture of Rumex
595 and Urtica under a mixture of weather conditions, unlike those studies.

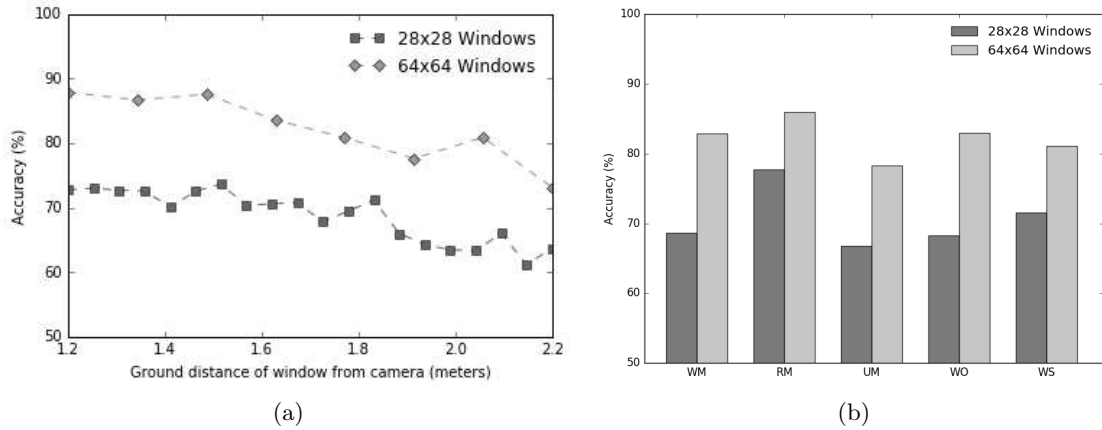


Figure 7: **Effects of distance, weed type and weather.** a) Classification performance of LBP\SVM as a function of the distance from the robot cameras (experiments on grass vs mixed weeds, mixed weather). b) Classification performance of LBP\SVM as a function of weed type (W: mixed weeds, R: Rumex, U: Urtica) and weather type (M: Mixed weather, O: Overcast, S: Sunny).

596 Results of the weed type and weather experiments are shown in 7b, again using the LBP\SVM
597 method. Here W stands for mixed weeds, R stands for Rumex and U stands for Urtica; M
598 stands for mixed weather, O stands for overcast weather and S stands for sunny weather.
599 Rumex classification was more accurate than Urtica or mixed weed classification, and mixed
600 weed classification was better than Urtica classification. For 28^2 pixel windows classification
601 under sunny weather conditions was better than classification under overcast weather conditions.
602 For 64^2 pixel windows the opposite weather pattern was found.
603 Finally, table 4 gives the results of applying the B\K\SVM classification method on full sized
604 (600×700) windows for data sets containing grass vs mixed and individual weed types under
605 mixed weather conditions. Again Rumex classification was the most accurate (97.9%), while
606 Urtica classification was the least accurate (94.65%).

607 Table 4: Results of applying the B\K\SVM method to full sized (600×700) windows (mixed
608 and individual weed types, mixed weather).

Experiment	Accuracy	Optimum K	Optimum C	Optimum γ
WM	95.1	16	2^{-3}	2^3
RM	97.9	19	2^{11}	2^1
UM	94.65	28	2^1	2^3

609 4 Conclusion

610 For our data set and the requirements upon which it is based, the best performing method
611 for the overall spray/no-spray decision is Linear Binary Patterns with Support Vector Machine
612 classification on 64^2 pixel windows.

613 LBPs are texture-based, rather than shape-based, features, and SVM is a highly nonlinear
614 model. This suggests that when a mixture of Rumex and Urtica is present and spray/no-spray
615 decisions are required, texture is more informative than shape, and that the discriminating
616 distribution of texture features has some nonlinear component. In particular, linear classification
617 of the same features with LDA performs less well.

618 All the accuracies in our independent re-implementations are lower than those reported in
619 the papers which originally proposed them. This may be due to several factors. First, our
620 data is more difficult to classify, even by human eye, than data used in the original studies.
621 Apart from [2], previous work has used vertical, downward-pointing cameras giving clear and
622 equal views of each point on the ground by removing the need for perspective correction. Our
623 data is more challenging, requiring additional invariance to perspective distance due to the
624 requirement to operate with cameras mounted on top of robot bodies rather than protruding
625 from them. Second, we required our data to come from a moving vehicle without expensive
626 image stabilisation, so intentionally included some blurred images which confuse edge-based
627 detection methods in particular, as these edges become blurred and no longer trigger these
628 detectors. Third, our data is required to come from a wide mixture of lighting and weather
629 conditions as would be encountered in real-world applications. Fourth, we did not allow fitting
630 of any parameters to the test set, and allowed each algorithm to see the test data only once, and
631 report only these results. Fifth, we have removed all possible experimenter, data set selection,
632 and publication bias by operating as an independent controlled study rather than setting out
633 to show the benefits of any one method.

634 For some applications, such as treatment by individual species-selective herbicides, finer classi-
635 fication of weed type into Rumex and Urtica may be required. Correct classification of Urtica
636 is harder to achieve than of Rumex, using the overall best LBP-SVM method. This is likely
637 because Rumex has larger, flatter leaves which present more obvious differences to most features
638 than Urtica's smaller and more contoured leaves. The BRISK-KMEANS-SVM method shows

639 less difference in performance between Urtica and Rumex when run on very large windows, as
640 expected this may be due to its ability to pick up the jagged edges of Urtica leaves. However
641 it does not work well for the regular 64^2 and 28^2 pixel windows, because it depends on the
642 ability to select good interest points from a large image. With 64^2 pixels the choice of interest
643 points is very limited and with 28^2 is almost non-existent, resulting in few or no interest points
644 being found to classify. LBP and BRISK are closely related, with LBP viewable as a special
645 case of BRISK that treats *every* pixel as an interest point and forces it to be included in the
646 classification, which explains why LBP outperforms BRISK for the smaller windows. The fact
647 that Rumex is in general easier to classify than Urtica may explain the existence of the many
648 more published method-proposing studies of Rumex vision than Urtica vision.

649 Evidence for the contribution of perspective effects to reducing accuracy is given by the distance
650 experiment result, which shows a considerable drop in accuracy as a function of distance from the
651 camera. If all plants were part of a perfectly flat ground surface then the affine transformation
652 would yield identical images to those taken by a vertical overhead camera as used in previous
653 studies. However real plants and ground are not flat and in particular the vertical structure
654 of plants near the camera results in them being enlarged out of proportion by the perspective
655 transform. The distortion is tolerable for short distances but makes the system less useful beyond
656 distances of around 1.5m. This suggests that for robots that are not able to mount vertical
657 overhead cameras, for example rough terrain specialist robots for which it is undesirable to have
658 overhanging parts that could be damaged by collisions, it may be preferable to concentrate visual
659 processing power only on nearby regions of ground space. Computation is a limited resource
660 for most mobile robots, which must trade off frame rate for size of spatial area to process and
661 battery power consumption. Designers of these robots should consider increasing frame rates
662 to obtain multiple views of the same nearby terrain up to around 1.5m away, at the expense of
663 ignoring further away terrain. It is possible that some improvements to distant recognition will
664 be possible using higher resolution cameras, to produce less pixel distortion during dewarping;
665 by using cameras with smaller apertures to gain deeper depth of field; and/or by mounting
666 cameras at higher positions such as one pole above the robot.

667 The effect of weather conditions on classification appears somewhat ambiguous from the tests
668 conducted here. The classifiers were trained on mixed sunny and overcast data, then tested on
669 mixed, sunny-only and overcast-only data. Overcast weather yields mostly diffuse lighting from

670 the whole sky, while sunny weather comprises mostly directional light from the sun’s position
671 in the sky, which gives rise to distinct shadows. In some cases the shapes of shadows may assist
672 classification (eg. the shapes of *Urtica* leaf shadows include the same distinctive jagged edges
673 as the leaves themselves), while in other cases shadows may act as noise over the features of the
674 real leaves. There is no clear contributing weather factor to these results, unlike the weed type
675 breakdown which gave clear evidence that *Urtica* are more responsible than *Rumex* for lowering
676 performance. Future work could try training classifiers on sunny-only and on overcast-only
677 data, or on more nuanced partitions of weather type, and test them on matched conditions.
678 However unlike the present experiment, this would require online robots to first classify the
679 overall weather condition in order to choose which classifier to use, which introduces further
680 complexity.

681 More fine grained weather and time-of-day classifications could be made. These can affect both
682 the spectrum of light illuminating the plants, and how the light interacts with the plants, for
683 example casting shadows, or cases of viewing low sunlight through leaves. The current dataset
684 contains time-of-day information which could be used to break down performance in this way;
685 epochs might also be further sub-classified into more detailed weather conditions, or more epochs
686 obtained from new weather and time-of-year conditions. The data sets are all collected from
687 the same weeds plots, and while we have argued that these do produce substantial variation
688 in the images, it would be useful to validate the methods on completely separate plots in the
689 future.

690 Window size is obviously an important factor on accuracy, because larger windows contain more
691 information than smaller ones. However there is a trade off because they represent larger spatial
692 regions which reduce the available accuracy of precision spraying. Robot designers can choose
693 between 83% accuracy at 106mm resolution, or 72% accuracy at 56mm resolution, from the
694 present studies. Very large windows can give near-perfect results as in the large-window BRISK
695 experiments yielding 95% accuracy for mixed weeds and 97.9% accuracy for *Rumex*. In practice
696 of course, classifications of single windows are unlikely to take place completely independently
697 of one another. Rather, in the field, a live robot would perform both spatial averaging of
698 neighbouring window classes, as well as temporal averaging as multiple images of the same
699 regions are taken over time from moving robot locations, for example via Markov Random
700 Fields as in [18], which would improve accuracy. The windows used here are non-overlapping

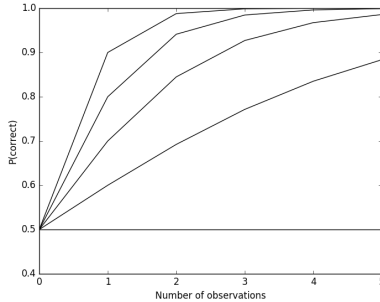


Figure 8: **Multi-observation fusion.** Showing the effect of Bayes-fusing multiple observations of a window. A live moving robot is likely to make several observations and classifications of each window from different poses, which when fused together will increase accuracy. Each line represents fusion of n observations of equal accuracy, whose per-observation accuracy is seen in the ‘number of observations = 1’ case ranging from 0.5 to 0.9 in steps of 0.1.

701 and live robots could further make use of overlapping windows to provide additional information
702 about the spatial frequencies across window boundaries that is not used in the present study. An
703 indication of the strength of accuracy amplification by multi observation fusion (which could be
704 temporal or spatial or both) is shown in fig. 8. This shows that the present LBP-SVM accuracy
705 is easily amplified into the mid or high 90s percentages by 2 to 5 observations, as could be
706 obtained by a moving robot. This is computed by Bayes-fusing accuracies with themselves
707 repeatedly, where the Bayesian fusion of two evidence probabilities p and q is given by,

$$\frac{pq}{pq + (1 - p)(1 - q)} \quad (18)$$

708 It can be seen from fig. 8 that fused data from two or three windows, observed over time
709 and/or space, is sufficient to bring most methods to 95%+ accuracy which is generally sufficient
710 (e.g. [34]) for spraying use in the field.

711 Running multiple classifiers and combining their results with an LDA meta-classifier yields a
712 slightly higher accuracy than pure LBP-SVM. The effect is only slight because all the feature-
713 classifier methods mostly work with similar image information to each other, with varying
714 levels of success, rather than working with different types of information. This information is
715 presumably Fourier or wavelet-like, and mostly linear, though with some nonlinearities which
716 enable the nonlinear SVM to outperform the other methods. All of the classification methods
717 tested here run comfortably in real time for live use, however running them all simultaneously
718 for meta-classification on a mobile robot platform would likely require parallel processors which

719 consume additional and valuable battery power.

720 As part of this publication we are making our training and test sets available for non-commercial
721 research by others under Creative Commons licence CC BY-NC 3.0 US. We hope that the
722 standardised setup presented here will enable performance to be improved upon through fair
723 evaluation of new methods and implementations, and though other researchers adding data
724 from new conditions to the set.

725 **References**

- 726 1. Motilal Agrawal, Kurt Konolige, and Morten Rufus Blas. Censure: Center surround ex-
727 tremas for realtime feature detection and matching. In European Conference on Computer
728 Vision, pages 102–115. Springer, 2008.
- 729 2. Faisal Ahmed, Md Hasanul Kabir, Shayla Bhuyan, Hossain Bari, and Emam Hossain.
730 Automated weed classification with local pattern-based texture descriptors. Int. Arab J.
731 Inf. Technol., 11(1):87–94, 2014.
- 732 3. T Anken, M Holpp, W Venn, HJ Kutterer, et al. Automatic detection of broad-leaved
733 dock in grassland. In International Conference on Agricultural Engineering-AgEng 2010:
734 towards environmental technologies, Clermont-Ferrand, France, 6-8 September 2010.
735 Cemagref, 2010.
- 736 4. Avital Bechar and Clément Vigneault. Agricultural robots for field operations: Concepts
737 and components. Biosystems Engineering, 149:94–111, 2016.
- 738 5. José M Bernardo and Adrian FM Smith. Bayesian theory, 2001.
- 739 6. Simon Blackmore, Bill Stout, Maohua Wang, and Boris Runov. Robotic agriculture—the
740 future of agricultural mechanisation. In Proceedings of the 5th European Conference on
741 Precision Agriculture, pages 621–628, 2005.
- 742 7. James S Cope, David Corney, Jonathan Y Clark, Paolo Remagnino, and Paul Wilkin.
743 Plant species identification using digital morphometrics: A review. Expert Systems with
744 Applications, 39(8):7562–7573, 2012.

- 745 8. Thomas G Dietterich. Ensemble methods in machine learning. In International workshop
746 on multiple classifier systems, pages 1–15. Springer, 2000.
- 747 9. Pedro Domingos. Bayesian averaging of classifiers and the overfitting problem. In ICML,
748 volume 2000, pages 223–230, 2000.
- 749 10. L Dürr, T Anken, H Bollhalder, J Sauter, KG Burri, and D Kuhn. Machine vision
750 detection and microwave based elimination of rumex obtusifolius l. on grassland. In 5th
751 European Conference on Precision Agriculture, Uppsala, Sweden, page 5, 2005.
- 752 11. Jerome Friedman, Trevor Hastie, and Robert Tibshirani. The elements of statistical
753 learning, volume 1. Springer series in statistics Springer, Berlin, 2001.
- 754 12. Steffen Gebhardt, Jürgen Schellberg, Reiner Lock, and Walter Kühbauch. Identifica-
755 tion of broad-leaved dock (rumex obtusifolius l.) on grassland by means of digital image
756 processing. Precision Agriculture, 7(3):165–178, 2006.
- 757 13. Lei Guo and Qingshan Li. Lbp and its variations for image classification. In Proceedings
758 of the 2012 International Conference on Electronics, Communications and Control, pages
759 712–715. IEEE Computer Society, 2012.
- 760 14. Esmael Hamuda, Martin Glavin, and Edward Jones. A survey of image processing tech-
761 niques for plant extraction and segmentation in the field. Computers and Electronics in
762 Agriculture, 125:184–199, 2016.
- 763 15. Dong-Chen He and Li Wang. Texture unit, texture spectrum, and texture analysis. IEEE
764 transactions on Geoscience and Remote Sensing, 28(4):509–512, 1990.
- 765 16. Geoffrey E Hinton, Simon Osindero, and Yee-Whye Teh. A fast learning algorithm for
766 deep belief nets. Neural computation, 18(7):1527–1554, 2006.
- 767 17. S Hiremath, G Van der Heijden, FK Van Evert, and A Stein. The role of textures to
768 improve the detection accuracy of rumex obtusifolius in robotic systems. Weed research,
769 52(5):430–440, 2012.
- 770 18. Santosh Hiremath, Valentyn A Tolpekin, Gerie van der Heijden, and Alfred Stein. Seg-
771 mentation of rumex obtusifolius using gaussian markov random fields. Machine vision
772 and applications, 24(4):845–854, 2013.

- 773 19. Chih-Wei Hsu, Chih-Chung Chang, Chih-Jen Lin, et al. A practical guide to support
774 vector classification. Tech. report, <https://www.csie.ntu.edu.tw/~cjlin/>, 2003.
- 775 20. Stefan Leutenegger, Margarita Chli, and Roland Y Siegwart. Brisk: Binary robust in-
776 variant scalable keypoints. In 2011 International conference on computer vision, pages
777 2548–2555. IEEE, 2011.
- 778 21. Cheryl McCarthy, Steven Rees, and Craig Baillie. Machine vision-based weed spot spray-
779 ing: a review and where next for sugarcane? In Proceedings of the 32nd Annual
780 Conference of the Australian Society of Sugar Cane Technologists (ASSCT 2010), vol-
781 ume 32, pages 424–432. Australian Society of Sugar Cane Technologists, 2010.
- 782 22. Geoffrey McLachlan. Discriminant analysis and statistical pattern recognition, volume
783 544. John Wiley & Sons, 2004.
- 784 23. D Moshou, D Kateris, XE Pantazi, and I Gravalos. Crop and weed species recognition
785 based on hyperspectral sensing and active learning. In Precision agriculture13, pages
786 555–561. Springer, 2013.
- 787 24. Xanthoula-Eirini Pantazi, Dimitrios Moshou, and Cedric Bravo. Active learning system
788 for weed species recognition based on hyperspectral sensing. Biosystems Engineering,
789 2016.
- 790 25. Akash Patel, DR Kasat, Sanjeev Jain, and VM Thakare. Performance analysis of various
791 feature detector and descriptor for real-time video based face tracking. International
792 Journal of Computer Applications, 93(1), 2014.
- 793 26. Gerassimos G Peteinatos, Martin Weis, Dionisio Andújar, Victor Rueda Ayala, and
794 Roland Gerhards. Potential use of ground-based sensor technologies for weed detection.
795 Pest management science, 70(2):190–199, 2014.
- 796 27. Gerrit Polder, Frits K van Evert, Arjan Lamaker, Arjan De Jong, GWAM Van der Hei-
797 jden, LAP Lotz, T Van der Zalm, and C Kampenaar. Weed detection using textural
798 image analysis. Plant Research International, PO Box, 16:6700, 2007.
- 799 28. Robert Rosenthal. The file drawer problem and tolerance for null results. Psychological
800 bulletin, 86(3):638, 1979.

- 801 29. Dejan ŠEATOVIĆ. 3d-object recognition, localization and treatment of Rumex obtusi-
802 folius in its natural environment. In 1 st International Conference on Machine Control &
803 Guidance, page 169, 2008.
- 804 30. Dejan Šeatović, Hansjörg Kutterer, and Thomas Anken. Automatic weed detection and
805 treatment in grasslands. In ELMAR, 2010 PROCEEDINGS, pages 65–68. IEEE, 2010.
- 806 31. Muhammad Hameed Siddiqi, Irshad Ahmad, and Suziah Bt Sulaiman. Weed recognition
807 based on erosion and dilation segmentation algorithm. In 2009 International Conference
808 on Education Technology and Computer, pages 224–228. IEEE, 2009.
- 809 32. ND Tillett, John A Marchant, and A Hague. Autonomous plant scale crop protection.
810 AgEng96, European Society of Agricultural Engineers A, 96:23–26, 1996.
- 811 33. FK Van Evert, G Polder, GWAM Van Der Heijden, C Kempenaar, and LAP Lotz.
812 Real-time vision-based detection of rumex obtusifolius in grassland. Weed Research,
813 49(2):164–174, 2009.
- 814 34. Frits K van Evert, Joost Samsom, Gerrit Polder, Marcel Vijn, Hendrik-Jan van Dooren,
815 Arjan Lamaker, Gerie WAM van der Heijden, Corné Kempenaar, Ton van der Zalm, and
816 Lambertus AP Lotz. A robot to detect and control broad-leaved dock (rumex obtusifolius
817 l.) in grassland. Journal of Field Robotics, 28(2):264–277, 2011.
- 818 35. Vladimir Vapnik. The nature of statistical learning theory. Springer Science & Business
819 Media, 2013.
- 820 36. Anup Vibhute and SK Bodhe. Applications of image processing in agriculture: a survey.
821 International Journal of Computer Applications, 52(2), 2012.
- 822 37. Luc Vincent and Pierre Soille. Watersheds in digital spaces: an efficient algorithm
823 based on immersion simulations. IEEE transactions on pattern analysis and machine
824 intelligence, 13(6):583–598, 1991.
- 825 38. Els Vrindts and Josse De Baerdemaeker. Optical weed detection and evaluation using
826 reflection measurements. In Photonics East (ISAM, VVDC, IEMB), pages 279–289. In-
827 ternational Society for Optics and Photonics, 1999.

828 39. Eric W Weisstein. Fast fourier transform. Wolfram World of Mathematics (online
829 resource), 2015.

830 Appendix

831 Here we give the intermediate results used for the parameter optimisation stage of classification
 832 for all 12 methods when trained on hyper-training and tested on hyper-test datasets containing
 833 grass vs mixed weeds under mixed weather conditions. This gives an indication of the effect of
 834 hyper-parameter optimisation on performance.

835 Tables 5 and 12 give the results for all classification methods except those involving the NN
 836 classifier (results for the NN classifier are given in the text) used on 28^2 pixel windows. 'nan'
 837 indicates an experiment abandoned due to unreasonable computation time, while NA stands
 838 for 'not applicable'. Tables 13 and 20 give the equivalent results for 64^2 pixel windows. For
 839 LBP>SVM, tables 5 and 13 give the results for the first stage of hyper-parameter optimisation,
 840 in which the hyper-parameters of the SVM C and γ were optimised. The second stage of
 841 optimisation for this method yielded optimised values for the hyper-parameters of the LBP
 842 ($n_{\text{points}}=20, r=5, \text{accuracy}=72.50\%$ for 28^2 pixel windows, $n_{\text{points}} = 24, r=4, \text{accuracy}=88.00\%$
 843 for 64^2 pixel windows). For LBP>NN, optimised parameters for the LBP were $n_{\text{points}} = 2, r = 4$
 844 for 28^2 pixel windows and $n_{\text{points}} = 10, r = 12$ for 64^2 pixel windows. For B)K>NN, the optimal
 845 value of K for the B)K method of feature extraction was 17 for 28^2 pixel windows and 18 for
 846 64^2 pixel windows. For FT>NN there were no parameters to optimise. For W>NN, the optimal
 847 value of d_{min} for the W method of feature extraction was $[1, \dots, 10]$ for 28^2 pixel windows and
 848 $[1, \dots, 5]$ for 64^2 pixel windows.

849 Table 5: Results for the classification method LBP>SVM with hyper-training and hyper-test
 datasets, on 28^2 pixel windows.

Kernel	Shrinking	Accuracy(%)	Optimum C	Optimum γ
linear	off	65.6	2^{11}	NA
linear	on	65.6	2^{11}	NA
rbf	off	68.3	2^{13}	2^{-1}
rbf	on	68.4	2^{13}	2^{-1}

851 Table 6: Results for the classification method B)K>SVM with hyper-training and hyper-test
 datasets, on 28^2 pixel windows.

Kernel	Shrinking	Accuracy	Optimum K	Optimum C	Optimum γ
linear	off	53.1	4	2^{-5}	NA
linear	on	53.1	4	2^{-5}	NA
rbf	off	53.1	4	2^{-5}	2^{-15}
rbf	on	52.5	4	2^{-5}	2^{-15}

852

Table 7: Results for the classification method FT)SVM with hyper-training and hyper-test datasets, on 28^2 pixel windows.

853

Kernel	Shrinking	Accuracy(%)	Optimum C	Optimum γ
linear	off	67.1	2^3	NA
linear	on	67.1	2^3	NA
rbf	off	69.3	2^1	2^3
rbf	on	69.4	2^1	2^3

854

Table 8: Results for the classification method W)SVM with hyper-training and hyper-test datasets, on 28^2 pixel windows.

855

Kernel	Shrinking	Accuracy (%)	d_{\min}	Optimum C	Optimum γ
linear	off	65.7	[1, ..., 9]	2^3	NA
linear	on	65.7	[1, ..., 9]	2^3	NA
rbf	off	66.6	[1, ..., 11]	2^{15}	2^{-3}
rbf	on	66.7	[1, ..., 11]	2^{15}	2^{-3}

856

Table 9: Results for the classification method LBP)LDA with hyper-training and hyper-test datasets, on 28^2 pixel windows.

857

Solver	Shrinkage	Accuracy(%)	Optimum n	Optimum r
svd	off	67.6	28	3
lsqr	off	67.6	28	3
lsqr	on	67.6	28	4
eigen	on	67.6	28	3

858

Table 10: Results for the classification method B)K)LDA with hyper-training and hyper-test datasets, on 28^2 pixel windows.

859

Solver	Shrinkage	Accuracy	Optimum K
svd	off	54.3	4
lsqr	off	54.1	23
lsqr	on	54.9	20
eigen	on	54.9	23

860

861 Table 11: Results for the classification method FT)LDA with hyper-training and hyper-test datasets, on 28^2 pixel windows.

Solver	Shrinkage	Accuracy(%)
svd	off	65.5
lsqr	off	65.5
lsqr	on	65.6
eigen	on	65.4

863 Table 12: Results for the classification method W)LDA with hyper-training and hyper-test datasets, on 28^2 pixel windows.

Solver	Shrinkage	Accuracy	d_{\min}
svd	off	63.1	[1, ..., 5]
lsqr	off	56.5	[1]
lsqr	on	63.3	[1, ..., 5]
eigen	on	nan	nan

865 Table 13: Results for the classification method LBP)SVM with hyper-training and hyper-test datasets, on 64^2 pixel windows.

Kernel	Shrinking	Accuracy(%)	Optimum C	Optimum γ
linear	off	80	2^5	NA
linear	on	80	2^5	NA
rbf	off	82	2^9	2^3
rbf	on	82	2^9	2^3

867 Table 14: Results for the classification method B)K)SVM with hyper-training and hyper-test datasets, on 64^2 pixel windows.

Kernel	Shrinking	Accuracy	Optimum K	Optimum C	Optimum γ
linear	off	59	17	2^3	NA
linear	on	61.25	17	2^5	NA
rbf	off	68.5	17	2^1	2^8
rbf	on	63	17	2^3	2^3

869 Table 15: Results for the classification method FT)SVM with hyper-training and hyper-test datasets, on 64^2 pixel windows.

Kernel	Shrinking	Accuracy(%)	Optimum C	Optimum γ
linear	off	76.5	2^5	NA
linear	on	76.5	2^5	NA
rbf	off	79	2^3	2^1
rbf	on	79	2^3	2^1

870

Table 16: Results for the classification method W)\SVM with hyper-training and hyper-test datasets, on 64^2 pixel windows.

871

Kernel	Shrinking	Accuracy (%)	d_{\min}	Optimum C	Optimum γ
linear	off	72.5	[1, ..., 10]	2^{13}	NA
linear	on	72.5	[1, ..., 10]	2^{13}	NA
rbf	off	76.5	[1, ..., 10]	2^{11}	2^3
rbf	on	76.5	[1, ..., 10]	2^{11}	2^3

872

Table 17: Results for the classification method LBP)\LDA with hyper-training and hyper-test datasets, on 64^2 pixel windows.

873

Solver	Shrinkage	Accuracy(%)	Optimum n	Optimum r
svd	off	81.5	28	4
lsqr	off	81.5	28	4
lsqr	on	82	16	4
eigen	on	81.5	16	4

874

Table 18: Results for the classification method B)\K)\LDA with hyper-training and hyper-test datasets, on 64^2 pixel windows.

875

Solver	Shrinkage	Accuracy	Optimum K
svd	off	76.5	20
lsqr	off	77.5	17
lsqr	on	78	17
eigen	on	77.5	22

876

Table 19: Results for the classification method FT)\LDA with hyper-training and hyper-test datasets, on 64^2 pixel windows.

877

Solver	Shrinkage	Accuracy(%)
svd	off	55.5
lsqr	off	53
lsqr	on	61
eigen	on	62

878

879 Table 20: Results for the classification method W)LDA with hyper-training and hyper-test datasets, on 64^2 pixel windows.

Solver	Shrinkage	Accuracy	d_{\min}
svd	off	67	[1, ..., 15]
lsqr	off	57	[1, ..., 13]
lsqr	on	66.5	[1, ..., 13]
eigen	on	nan	nan

880